Materials Letters 67 (2012) 67–69

Contents lists available at SciVerse ScienceDirect

Materials Letters

journal homepage: www.elsevier.com/locate/matlet

Dislocations in $Bi_{0.4}Ca_{0.6}MnO_3$ epitaxial film grown on (110) $SrTiO_3$ substrate

Y.H. Ding [a], R.S. Cai [a], Y.Q. Wang [a,*], Y.Z. Chen [b], J.R. Sun [b]

[a] The Cultivation Base for State Key Laboratory, Qingdao University, No. 308 Ningxia Road, Qingdao, 266071, PR China
[b] State Key Laboratory of Magnetism and Beijing National Laboratory for Condensed Matter Physics, Institute of Physics, Chinese Academy of Sciences, Beijing, 100080, PR China

ARTICLE INFO

Article history:
Received 2 April 2011
Accepted 6 September 2011
Available online 10 September 2011

Keywords:
Thin film
Epitaxial growth
Electron microscopy
Defects

ABSTRACT

$Bi_{0.4}Ca_{0.6}MnO_3$ (BCMO) film with a thickness of 110 nm was epitaxially grown on a (110) $SrTiO_3$ (STO) substrate using pulsed laser ablation technique. The microstructure of the epitaxial films was investigated by transmission electron microscopy (TEM) and high-resolution transmission electron microscopy (HRTEM) in details. Two different kinds of dislocations, one being perpendicular to the BCMO/STO interface, the other being parallel to the interface, have been commonly observed. The formation mechanism for these dislocations has been discussed. All the dislocations are thought to relieve the local strain in the epitaxial film.

1. Introduction

Perovskite manganites of the formula $R_{1-x}A_xMnO_3$ (R being a trivalent rare earth and A being a divalent alkaline-earth ion) have attracted great attention recently due to their wide variety of electronic, magnetic, and structural states, and the coexisted and competitive mechanisms associated with the strong coupling among the spin, charge and orbital degrees of freedom [1,2]. These materials are sensitive to magnetic, electric fields, pressure, and X-ray/visible light irradiation [3,4]. The charge- and orbital-ordered (CO/OO) state in perovskite manganites has aroused a lot of interest for its colossal response to external stimuli.

$Bi_{1-x}Ca_xMnO_3$ is a particularly interesting material. Its transition temperature for the charge and orbital ordering is very high, well above the room temperature, which makes careful investigation of the transition behavior convenient [5]. $Bi_{1-x}Ca_xMnO_3$ was first studied by Bokov et al. [6], who presented detailed structural data on the series. Further details of magnetic and charge-ordered properties were investigated by Bao et al. [7] and Chen et al. [8]. For the epitaxial manganite films, the transition to the CO/OO state is strongly influenced by lattice strains. The relationship between epitaxial strain and phase transitions, such as the CO transition in $Bi_{0.4}Ca_{0.6}MnO_3$ (BCMO) thin films, has been the subject of numerous investigations [9–11]. As we all know, the microstructure and physical properties of materials have a close relationship. Therefore, it is imperative to obtain microstructural information of BCMO epitaxial films. However, to our knowledge, few reports concerning the microstructure, especially the information about the nature of defects in the BCMO epitaxial films can be found. In this Letter, we report on the transmission electron microscopy (TEM) studies of the linear defects, dislocations, in epitaxial BCMO film with a thickness of 110 nm grown on a (110) $SrTiO_3$ (STO) substrate by pulsed laser deposition (PLD). Two different kinds of pure edge dislocations in morphology, either perpendicular or parallel to the BCMO/STO interface, have been commonly observed. The formation mechanism of these dislocations is also discussed.

2. Experimental

Epitaxial BCMO films were prepared on a (110) STO substrate by PLD technique (laser wavelength = 248 nm, repetition rate = 5 Hz and fluency = 7 J/cm^2) from a target with a nominal composition of BCMO. During the deposition, the substrate temperature was kept at ~700 °C and the oxygen pressure at ~60 Pa. The film thickness is 110 nm, controlled by deposition time. Structural analyses of the films were performed by X-ray diffraction (XRD) on a Philips X'pert Pro diffractometer using Cu $K\alpha_1$ radiation. The surface morphology of the films was analyzed by atomic force microscopy (AFM) [Digital Instrument (DI) NanoScope IIIa].

Specimens for TEM examinations were prepared in a cross-sectional orientation ([1$\bar{1}$0] zone-axes for the STO substrates) using conventional techniques of mechanical polishing and ion thinning. The ion milling was performed using a Gatan Model 691 Precision Ion Polishing System (PIPS). The bright field (BF) imaging, selected-area electron diffraction (SAED) and high-resolution transmission electron microscopy (HRTEM) examinations were carried out using a JEOL JEM 2100F transmission electron microscope operating at 200 kV.

3. Results and discussion

Fig. 1 shows a typical XRD spectrum of the (110) and (220) reflections for the BCMO films. It can be seen that the (110) and (220)

* Corresponding author. Tel./fax: +86 532 83780318.
E-mail address: yqwang@qdu.edu.cn (Y.Q. Wang).

0167-577X/$ – see front matter © 2011 Elsevier B.V. All rights reserved.
doi:10.1016/j.matlet.2011.09.026

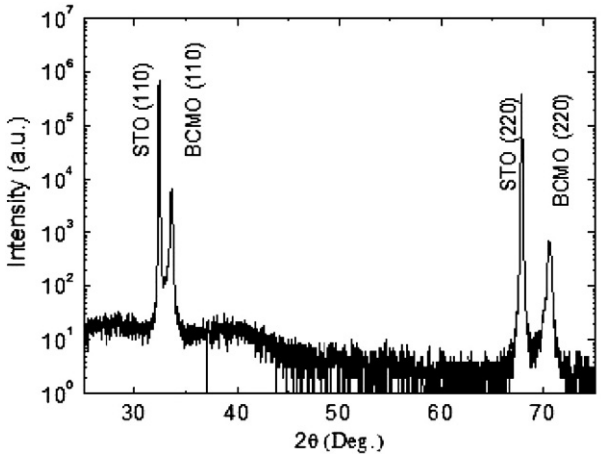

Fig. 1. XRD patterns for STO substrate and BCMO film.

peaks of the film are sharp, and very close to those of the substrates. This indicates the good epitaxial relationship between the film and the substrate. No peaks of secondary phase are observed, which indicates that the films are a single phase. What's more, the (110)-oriented substrate can bear the tensile stress and achieve good orientation growth. XRD data show that BCMO films grow in a cubic structure on STO substrates, with the epitaxial relationship of $(110)_{BCMO}//(110)_{STO}$.

Fig. 2(a) shows a typical $2\times2\ \mu m^2$ atomic force microscope image of the epitaxial BCMO film with a thickness of 110 nm. It is obvious that the surface morphology of the film exhibits a ridge-shaped structure along the [001] direction with an average column width of ~50 nm. The root mean square surface roughness was ~2.6 nm for the epitaxial film. The (110) film shows a good crystallinity, and the regular ridge-like stripes indicate it has a single domain structure. This result demonstrates the presence of a preferred growth direction for film deposited on the (110)-oriented STO substrate.

To obtain the microstructural information of the BCMO film, TEM and HRTEM are employed. Fig. 2(b) is a typical BF TEM image of a cross-sectional of the BCMO/STO sample. The BF image was taken under a two-beam condition with g = 110. It can be seen from Fig. 2(b) that there are darker regions near the BCMO/STO interface, which are caused by misfit dislocations. Fig. 2(c) is a typical SAED pattern taken from the epitaxial film region, which corresponds to a $[1\bar{1}0]$ zone-axis diffraction pattern of BCMO film, suggesting that the epitaxial BCMO films are good single crystals. Fig. 2(d) is a typical SAED pattern taken from the interface region between BCMO film and STO substrate. It showed a superposition of BCMO $[1\bar{1}0]$ and STO $[1\bar{1}0]$ zone-axis SAED patterns. The epitaxial BCMO film has an interface relationship of $(110)_{BCMO}//(110)_{STO}$ and $[\bar{1}11]_{BCMO}//[\bar{1}11]_{STO}$ with respect to the substrate.

Extensive HRTEM examinations of the BCMO epitaxial film show that two different kinds of pure edge dislocations commonly exist in the films, one being perpendicular to the interface, and the other being parallel to the interface. One example is shown in Fig. 3(a). Fig. 3(a) is a typical HRTEM image of the interface region between BCMO and STO, showing three pure edge dislocations. The three dislocations are indicated by D1, D2 and D3 in Fig. 3(a), respectively. The extra half atomic plane, which is a characteristic of a perfect dislocation, is indicated by dashed lines in Fig. 3(a). In order to show the extra half atomic planes more clearly, an enlarged HRTEM image of the three dislocations is shown in Fig. 3(b). For D1 and D2, the extra half planes are inserted from the direction parallel to the interface region, while D3, the extra half atomic plane is inserted from the direction perpendicular to the interface region. For D1, the extra half atomic plane is inserted from the left, while for D2, the extra half atomic plane is inserted from the right, so D1 is regarded as positive perfect dislocation, and D2 is considered to be a negative perfect dislocation. Fig. 3(c) shows the one dimensional Fourier filtered lattice image of Fig. 3(b) with the lattice planes parallel to the interface which is indicated by the dashed lines. It can be clearly seen that two extra half planes are inserted from the direction parallel to the interface, confirming that they are pure edge dislocations. To determine the Burgers vectors for D1 and D2, Burgers circuits are drawn for D1 and D2 as shown in Fig. 3(d). From Fig. 3(d), it can be clearly seen that there is a gap between the starting and ending points of the Burgers circuit, which is indicated by an arrow. The Burgers vectors for D1 and D2 are determined to be $\mathbf{b}=\langle001\rangle$, but they have opposite signs. The theoretical equilibrium configuration for the dislocations with the opposite signs is that the angle between the dislocation lines is 45° [12]. The Burgers vectors for D1 and D2 have opposite signs, if they are on the same gliding plane, they will attract each other until annihilation occurs. Here the dislocations D1 and D2 do not lie on the same gliding plane, so they will form an equilibrium configuration and the angle between the dislocation lines should be 45°. For D1 and D2, they form a dipole and are stable. Fig. 3(e) shows the one dimensional Fourier filtered lattice image of Fig. 3(b) with the lattice planes perpendicular to the interface which is indicated by the dashed lines. It can be clearly seen that one extra half plane is inserted from the direction perpendicular to the interface, confirming that it belongs to a pure-edge dislocation. To determine the Burgers vector for D3, Burgers circuit is drawn for D3 as shown in Fig. 3(f). From Fig. 3(f), we can clearly see a gap between the starting and ending points of the Burgers circuit, as indicated by an arrow. The Burgers vector for D3 is determined to be $\mathbf{b}=\langle110\rangle$.

The formation mechanism for these two pure-edge dislocations is different. For the dislocation parallel to the BCMO/STO interface, it was caused by the roughness of the substrate. As proved by the atomic force spectroscope analysis, the STO substrate is not smooth, with a root-mean square roughness of ~0.6 nm. Then STO substrate surface can be regarded to consist of steps or terraces. If the height of the step or terrace is equal to (1/2)c of BCMO, the domains grown on the terrace will be displaced by (1/2)c along the growth direction, compared with those neighboring grains grown on the normal surfaces. Consequently an antiphase boundary will form. This has been observed in the $Ba_{0.75}Sr_{0.25}TiO_3$ epitaxial film grown on a (001) $LaAlO_3$ substrate [13]. If the step height is not equal to (1/2)c of BCMO, dislocations parallel to the interface will be produced. The dislocations parallel to the interface have never been observed in

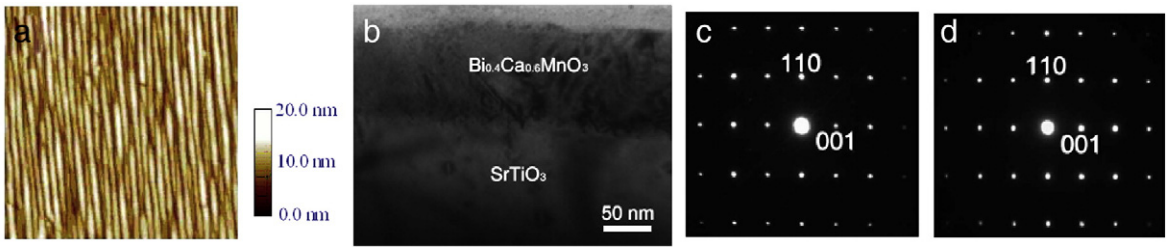

Fig. 2. (a) AFM image of epitaxial BCMO film; (b) cross-sectional BF image of BCMO/STO sample; (c) SAED pattern from the epitaxial film; (d) SAED pattern from the interface region.

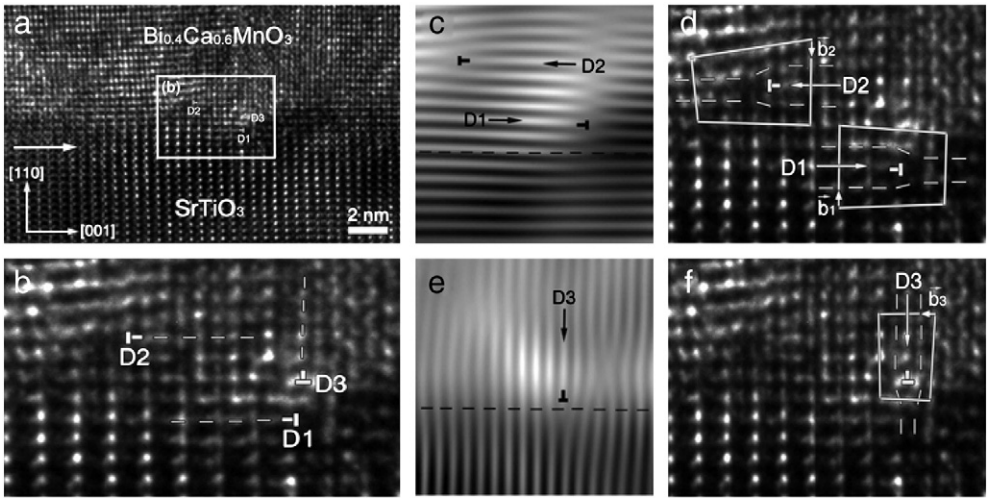

Fig. 3. (a) HRTEM of BCMO/STO interface region; (b) an enlarged HRTEM image of enclosed region in (a); (c) Fourier filtered lattice image of (b) along the direction parallel to the interface; (d) Burgers circuits for D1 and D2; (e) Fourier filtered lattice image of (b) along the direction perpendicular to the interface; (f) Burgers circuit for D3.

the epitaxial perovskite films before. In order to relieve the strain along the growth direction, dislocations with Burgers vectors of opposite signs will form in pairs, such as D1 and D2 in Fig. 3(a). However, for the dislocations perpendicular to the interface, they were caused by the lattice mismatch between the BCMO and STO. The formation of these dislocations will relieve the strain perpendicular to the growth direction in the epitaxial films. The films are grown in an island mode, and the two islands will coalesce as thickness increases [14]. The lattice strain will be accommodated by the elastic deformation if the film thickness is below 110 nm [14]. When the thickness exceeds 110 nm, the strain in the (110) epitaxial film cannot be released by elastic deformation. The BCMO film and STO substrate cannot match well along the direction perpendicular to the interface. Thus, mismatch dislocations will form.

4. Conclusions

In summary, BCMO films are a single phase and are epitaxially grown on (110) STO substrates. Dislocations both perpendicular and parallel to the interface have been observed in the epitaxial BCMO films. The dislocation parallel to the interface was caused by the roughness of the STO substrate. The dislocation perpendicular to the interface was produced by the lattice mismatch. All the dislocations could relieve the strain in the epitaxial films.

Acknowledgments

The authors would like to thank for the financial support from the National Natural Science Foundation of China (Grant nos. 10974105 and 50832007), National Basic Research of China (Grant no. 2007CB925002), the Project of Introducing Talents to Support Thousand Talents Programs (Grant no. P201101032), and the Program of Science and Technology in Qingdao City (Grant no. 11-2-4-23-hz), and the Scientific Research Starting Foundation for the Introduced Talents at Qingdao University (Grant no. 06300701). Y. Q. Wang would also like to thank for the financial support from Taishan Outstanding Overseas Scholar Program of Shandong Province.

References

[1] Chuang YD, Gromko AD, Dessau DS, Kimura T, Tokura Y. Science 2001;292:1509–13.
[2] Savosta MM, Novák P. Phys Rev Lett 2001;87(137204):1–4.
[3] Gunnarsson R, Ivanov ZG, Dubourdieu C, Roussel H. Phys Rev B 2004;69(054413):1–6.
[4] Miyano K, Tanaka T, Tomioka Y, Tokura Y. Phys Rev Lett 1997;78:4257–60.
[5] Woo H, Tyson TA, Croft M, Cheong S-W, Woicik JC. Phys Rev B 2001;63(134412):1–12.
[6] Bokov VA, Grigoryan NA, Bryzhina MF. Phys Stat Sol 1967;20:745–54.
[7] Bao W, Axe J, Chen C, Cheong S-W. Phys Rev Lett 1997;78:543–6.
[8] Chen YZ, Sun JR, Wang DJ, Liang S, Wang JZ, Han YN, et al. J Phys Condens Matter 2007;19(442001):1–6.
[9] Kim DH, Christen HM, Varela M, Lee HN, Lowndes DH. Appl Phys Lett 2006;88 (202503):1–3.
[10] Chen YZ, Sun JR, Liang S, Lv WM, Shen BG, Wu WB. J Appl Phys 2008;103 (096105):1–3.
[11] Chen YZ, Sun JR, Liang S, Lu WM, Shen BG. J Appl Phys 2008;104(113913):1–4.
[12] Wang YQ, Li T, Liang WS, Duan XF, Ross GG. Nanotechnology 2009;20(315704):1–4.
[13] Wang YQ, Liang WS, Petrov PK, Alford NM. Appl Phys Lett 2011;98(091910):1–3.
[14] Ding YH, Cai RS, Du QT, Wang YQ, Chen YZ, Sun JR. J Cryst Growth 2011;317:115–8.